Renewable infrastructure in a field of dunes: changes to near bed turbulence & sediments

C. Unsworth *School of Ocean Sciences, Bangor University, UK – christopher.unsworth@bangor.ac.uk*
M. A. Austin *School of Ocean Sciences, Bangor University, UK – m.austin@bangor.ac.uk*
K. Van Landeghem *School of Ocean Sciences, Bangor University, UK – k.v.landeghem@bangor.ac.uk*.
A. Couldrey *HR Wallingford, UK – a.couldrey@hrwallingford.com*
R. Whitehouse *HR Wallingford, UK – r.whitehouse@hrwallingford.com*

ABSTRACT: The world's shallow continental shelves are currently experiencing a rapid pace of development from the growth of offshore renewable energy. Our ability to predict the response to new seabed infrastructure is limited by our models of flow and sediment transport which were created and validated assuming a uniform flow structure. We present field results from a deployment in the eastern Irish Sea where profiles of flow and turbulence were measured and used to drive a range of suspended sediment models. The range of models, and the various ways of forcing them, are tested against measured suspended sediment concentrations from a calibrated multi-frequency acoustic backscatter system. It was found that the bed shear stress as measured via 2D depth averaged approximations (with velocities from a bed mounted ADCP), as well as the TKE method (from a near bed ADCP) was the most accurate, whilst law of the wall approximation performed poorly. We found that the method of Garcia and Parker (1992) family of methods produced the most accurate measure of suspended sediments. Transport near the threshold of motion (30% of measurements) was poorly represented by all combinations of methods. The highest suspended sediment concentrations (10% of measurements) were also poorly predicted, likely due to the changing bed level which occurred during these high concentration events.

1INTRODUCTION

The movement of sediment on the seabed is still one of the most challenging processes to accurately model and predict (Egan et al., 2019; Salim et al., 2018; Tang et al., 2019) (Dey et al., 2020; Tsai & Huang, 2019). One of the most pressing issues for predicting sediment transport in marine and coastal environments is understanding the effects of new offshore wind farm infrastructure on both the structure of the flow, the subsequent effect on sediment transport, and the change to the seabed.

A typical assumption when applying sediment transport models is the use of mean flow parameters, usually assuming the form of the turbulent boundary layer. The emplacement of new infrastructure on the seabed forms a natural laboratory for flow and sediment transport processes to be investigated, notably because of two effects: 1) the creation of a localised source of pressure drag and non-equilibrium turbulence and 2) the subsequent effect on the form of the seabed. These effects cause two main problems for estimating sediment transport: 1) localised turbulence generation lowers the bulk flow velocity and 2), localized sources of turbulence tend to generate non-equilibrium flow and sediment transport fields, which are not part of the assumptions in the sediment transport models.

Here we use a recently collected suite of acoustic data from a seabed lander deployed in a field of dunes which had a section of seabed electricity cable attached to it. We use the data to test a variety of methods for estimating bed shear stress and suspended sediment concentrations and ask which methods work well in this environment.

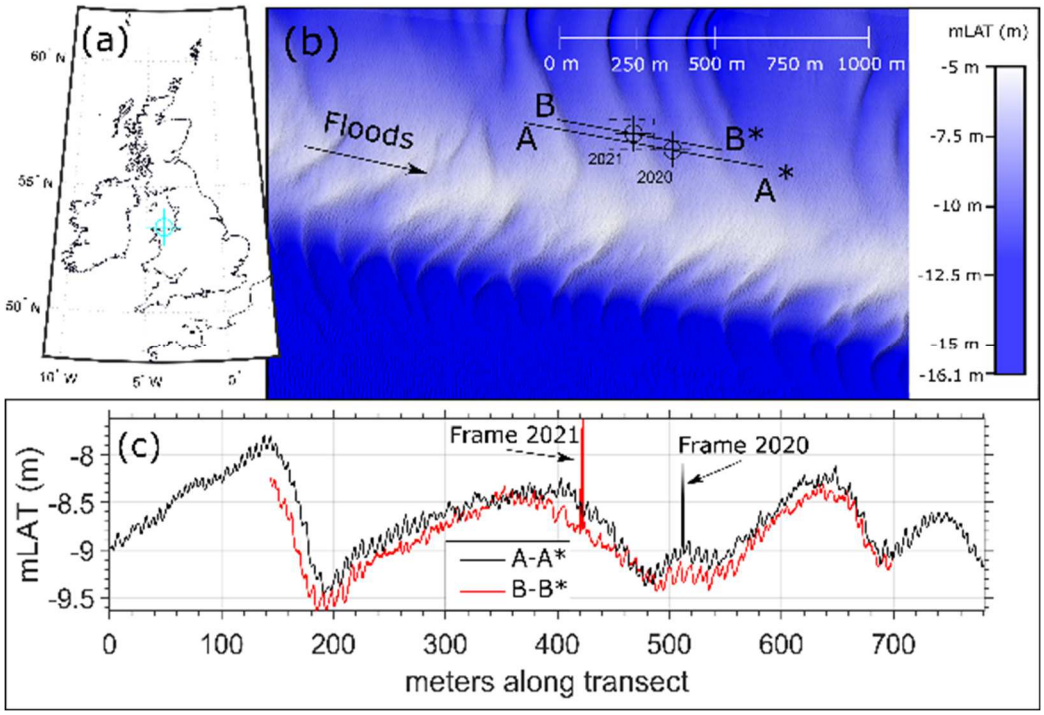

Figure 1. (a) location of site, (b) 2 m Bathymetry of "constable Bank", with instrument frame locations and bedform profiles highlighted. (c) location of frames and bedforms measured during the surveys.

2METHODS

2.1 Field Site

The study site was on the Constable Bank in the Irish Sea 6 km off the coast of North Wales, UK (53° 22.5616' N, 3° 43.6308' W, Figure 1, see end of document). This location is known to have active bedform migration and is close to existing and proposed offshore wind farms. The site has a semi-diurnal macro tidal regime, mean tidal ranges of 7.2 m at springs and 3.8 m at neaps (measured at Llandudno, https://ntslf.org). Dominant flood and ebb directions are 100° and 270 – 290°, respectively. Two separate field deployments were conducted, one in September 2020 and one in July 2021. Repeated vessel mounted Multibeam Echosounder (MBES) surveys were performed during the surveys to map bedform migration. Tides during the 2020 surveys were during the autumnal equinox and thus were some of the largest of the year, whilst tides during the 2021 surveys had an average tidal range for the site. Significant wave heights during the start of each deployment were 1 to 1.5 m high with 3 second periods, lowering to calm conditions towards the end of each deployment.

Grain size at the field site was measured from 11 Shipeck grab samples taken before deployments, was found to be a consistent uniform sand with a median grain size of 244 µm (Figure 2).

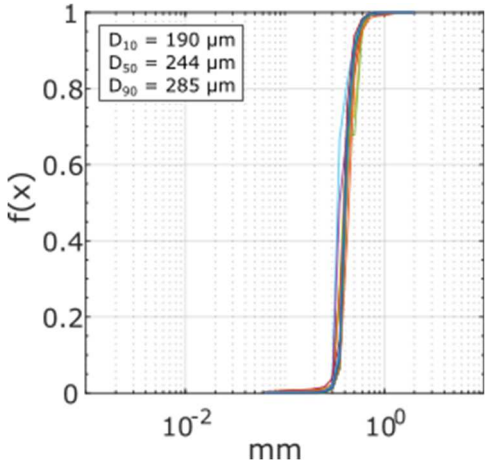

Figure 2. Grain size distributions of 11 grab samples from both surveys at the location of the instrument frames.

Thresholds of motion were calculated via the modified Shields curve (Soulsby, 1997):

$$D^* = D_{50}\left(\frac{(S-1)g}{\nu^2}\right)^{1/3} Eq.\ 1$$

$$\theta^*_{crit} = \frac{0.3}{1+1.2D^*} + 0.055(-0.02D^*) Eq.\ 2$$

$$\theta^*_{sus} = \frac{0.3}{1+D^*} + 0.1(-0.05D^*) Eq.\ 3$$

where D_{50} is the median grain diameter, g is the acceleration due to gravity, ν is the kinematic viscosity of the sea water (at 15°C, 1.1384 x10-6 m^2 s^{-1} and s = 2.58 for quartz grains in seawater.

2.2 Data collected

A suite of acoustic data was collected from a bespoke seabed lander which had a section of undersea electricity cable attached at one end (Figure 3). The data presented here are from AQD-1, the ABS, and the upward facing Sig1K.

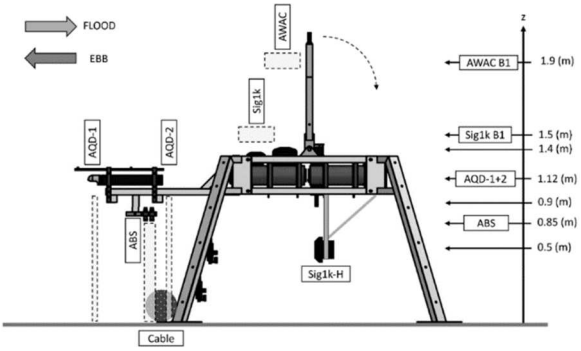

Figure 3. Schematic of the instrument lander. Dashed outlines indicate location of measurements used in the survey, "B1" indicates the location of the first bin of data. The section of cable is fixed to the base of the left side of the lander.

The combination of upward and downward facing ADCP's allows for the mean and near bed flow structure to be measured, including any effects from the bedforms on the flow field as well as the effects of the cable and instrument lander on the ebb tide velocities, especially near the bed. Standard thresholds for correlation and amplitude were set for ADCP's, which removed < 5% of data, velocity spikes were filtered out using a gradient threshold of 0.14 m s^{-2}. Removed values were replaced with linearly interpolated values, if the gap between good values was smaller than 4 data points. Velocities were collected in beam coordinates and converted in post processing. A local three-velocity component (UVW) coordinate system was applied using the median flood tide direction for each instrument, so that $\bar{U}$ is maximised and $\bar{V}$ over time is minimised, and were decomposed into burst-mean (with overbar) and turbulent components (with prime)

$$U = (\bar{U} + u')[v; w]. Eq.\ 4$$

3RESULTS

3.1 Bedforms

The seabed bathymetry at Constable Bank consists of sedimentary bedforms of two main scales. The larger scale bedforms in and around the lander site have an average length of 194 m by 0.94 m high (range from 0.8 – 1.5 m high, 200 – 300 m long), which have an orientation of 150° (Figure 1). Superimposed on these larger bedforms are smaller dunes of a scale 19 m long and 0.16 m high with a dominant angle of 100°, which is in line with the dominant flood tide direction. The location of the bedform crests changed less than 0.1 m between the surveys in 2020 and 2021. Their shape changed during the tides in a similar way to estuarine bedforms (Lefebvre et al., 2022). The size, shape and orientation of these smaller bedforms indicates there would be no/ or little significant flow separation from the larger host bedforms (Herbert et al., 2015). The height of the larger bedforms is roughly equal to the height of the instrument frame (1.4 m) so near bed and upward facing ADCP's will be measuring the turbulent boundary layer generated from the bedforms (Dyer, 1986; McLean et al., 1999; Nowell & Church, 1979).

3.2 Enhanced turbulence and suspended sediments

Given the directional setup of the experiment, we expect floods to have "natural" flows, whilst data collected during the ebb tides will also contain the turbulent wakes from the instrument frame and cable. The example profiles in Figure 4 are from the 2nd tide of the 2020 deployment and show the expected higher near-bed suspended sediment concentrations, and a steeper near bed velocity profile in ebbs.

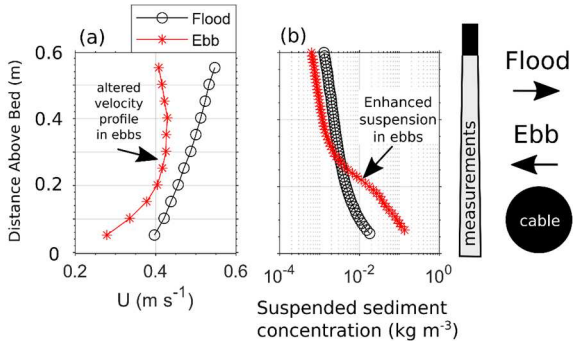

Figure 4. Examples of burst average (10 minute) velocity profiles (a) and suspended sediment concentrations (b). Flood tides measure "natural" flows whereas ebbs are affected by the instrument frame and electricity cable, illustrated on the right.

Such alteration of the near bed velocity profile should have affects on the estimating of bed shear stress via standard methods.

3.3 Estimating bed shear stress

For an estimate of bed shear stress using depth average properties, we used the 2D approximation with a Chezy coefficient (C') based on the bed sediment samples and flow depth (Baas et al., 2000; Van den Berg & Van Gelder, 1993):

$$\theta'_a = \frac{\rho_w \bar{U}^2}{(\rho_s - \rho_w)(C')^2 D_{50}} \quad Eq.\ 5$$

$$C' = 18\,log(\frac{4h}{D_{90}}) \quad Eq.\ 6$$

where ρ_w is the density of sea water, ρ_s is the density of the sediment, h is the flow depth. This method is the default for the 2D version of *Telemac*, for example. The method used in *MIKE21*, uses a manning's *M* for roughness:

$$\theta'_b = C\rho\bar{U}^2, \quad \text{Eq. 7}$$

$$C = \frac{g}{(Mh^{1/6})^2} \quad \text{Eq. 8}$$

where *M* was set to 32 $m^{1/3}s^{-1}$.

We calculate two estimates of bed shear stress suing the law of the wall (*LoW*) method, one with the upward facing ADCP (LoW_{Up}) and downward facing ADCP (LoW_{down}) via the usual equation:

$$u(z) = \frac{u_*}{\kappa}\left[ln\left(\frac{z-h}{z_0}\right)\right] \quad Eq.\ 9$$

Where u_* is the shear velocity, $\kappa = 0.41$ is the von Karmon constant, z is the vertical coordinate, z_0 is the roughness height, and bed shear stress is:

$$\tau_b = \rho u_*^2 \quad Eq.\ 10$$

this calculation was perfumed on the burst averaged by first selecting to lowest 5 velocities to regress, calculated the R^2, and if the fit was better than a set threshold ($R^2 = 0.85$), the next datapoint above was added to the regression until the threshold was passed. At which the previous iteration was used to get u_* and z_0. This procedure produced values for ~ 80 % of all measurements.

Alternatively, bed shear stress can be calculated from near bed turbulence data, which have been shown to perform well in complex flows where the assumptions in the law of the wall and 2D approximations are invalid (Biron et al., 2004; Kim et al., 2000; Pope et al., 2006; Williams et al., 1999).

Here we used the Reynolds Stressed based covariance method outlined by (Klipp, 2018):

$$TKE = \sqrt{\overline{u'w'}^2 + \overline{v'w'}^2} \quad Eq.\ 11$$

$$\tau_b = \sqrt{TKE} \quad Eq.\ 12$$

The TKE method outlined by via (Soulsby & Dyer, 1981):

$$TKE = 0.5\rho(\overline{u'^2} + \overline{v'^2} + \overline{w'^2}) \quad Eq.\ 13$$

$$\tau_b = 0.19TKE \quad Eq.\ 14$$

and the inertial dissipation method (Tennekes & Lumley, 1972)

$$u_* = (\varepsilon kz)^{1/3} \quad Eq.\ 15$$

Where dissipation (ε) can be calculated from (Scannell et al., 2017) for both tide and waves, and assuming a balance of production and dissipation.

The law of the wall-based methods shows by far the largest scatter for any value of $\bar{U}$ for either floods or ebbs (Figure 5a) – likely due to the presence of a turbulent wake in due to the bedforms on both phases of the tide or the extra effects of the wake from the cable and

instrument lander are present in the ebb tide. 2D-depth averaged methods show the least scatter due to their inputs having the least noise (Figurer 5a).

The turbulence-based methods of estimating u^* all produce different trends, but with roughly the same amount of scatter per value of $\overline{U}$. The *Klipp* method seems to perform worse in ebbs than floods, suggesting that the turbulence coming from the frame and cable are negatively affecting the results from this method. The TKE and dissipation-based method should produce similar values (assuming a balance between production and dissipation of turbulence) but it is clear that on both floods and ebbs the dissipation-based method consistently underpredicts u^* - possibly due to the amount of turbulence generated locally by the lander and the bedforms field.

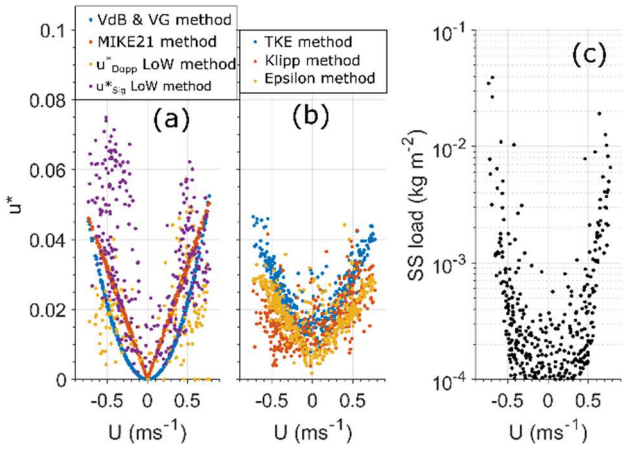

Figure 5 (a) and (b) display the variation of estimates for u* based upon the profile averaged mean velocity from the upward facing Sig1k and Law of the Wall method on the Sig1k and AQD-1 data (a), and (b) methods based upon turbulence Figure 5 (c) display measured suspended sediment loads from the ABS. $\overline{U} > 0$ = floods, < 0 = ebbs.

3.4 Estimating suspension

Next, we compare a range of methods for estimating near bed suspended sediment concentrations; the methods of: (Einstein, 1950; Rijn, 2007; Smith & McLean, 1977) and the (Garcia & Parker, 1991) "family" of methods (de Leeuw et al., 2020; Wright et al., 2005). We use the range of methods of estimating u^* outlined in section 3.3 to drive those models. We do this to try and get a measure of how good a measure of u^* is needed to predict suspended sediment concentrations in an environment where bedforms and infrastructure are on the seabed.

Regressions of observed and predicted near bed suspended sediment concentrations are shown in Figure 6 (at the end of the document). From these comparisons we suggest that the Garcia & Parker (1991) method, and its' decedents Wright et al., (2005) and de Leeuw et al., (2020) are the most sensible methods of estimating near bed suspended sediment concentration. All other methods show major differences in predicted vs measured concentrations at any value.

Plotting the distributions of predicted suspended sediment concentrations (Figure 7) allows a comparison of SSC methods and u^* methods to be compared at the same time. For example, if a SSC model was perfect, but the u^* data used was not, it would still not show the same distribution as the measured data. One key finding here is the highest and lowest concentrations are poorly predicted by any combination of methods.

Using the 2D methods with Garcia and Parker (1991) only *Eq.* 5-6 does well at the higher concentrations, but poorly for ~ 60% of the distribution, whilst *Eq. 7-8* performs well for 70 % of the distribution but the shape of the distribution at the high concentrations is poor. The TKE method has a better distribution at the higher concentrations and shows an excellent distribution down to 10^{-6} kg m^3, where the threshold of motion and the noise flood of the ABS begin to be reached.

The methods of Einstein, 1950; Rijn, 2007; Smith & McLean, 1977, appear to do well at the highest concentrations but considering that these models overpredict concentrations for the rest of the distribution, it seems likely that they provide the right results at high concentrations for the wrong reasons.

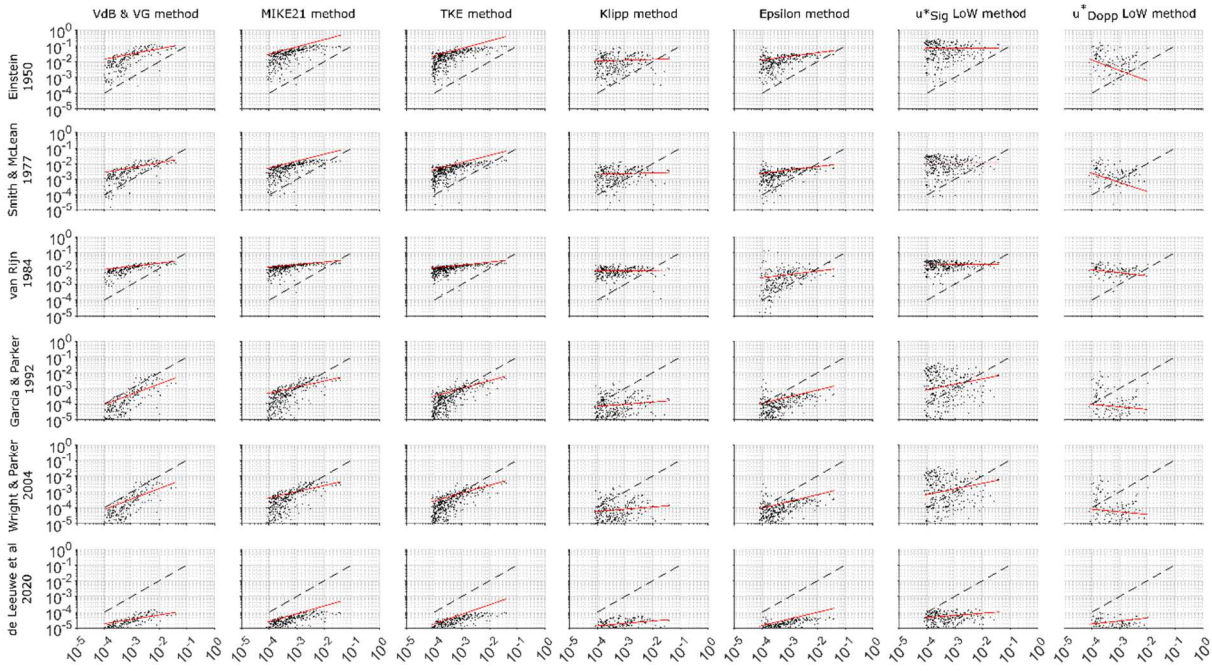

Figure 6. Comparisons between methods of estimating bear shear stress (right to left) and suspended sediment methods (top to bottom. X axis are measured values of SSC, Y axis is the predicted values. 1:1 slope is provided as a dashed line. Values are in log10 kg m-3. Red lines show a best fit from a robust linear regression.

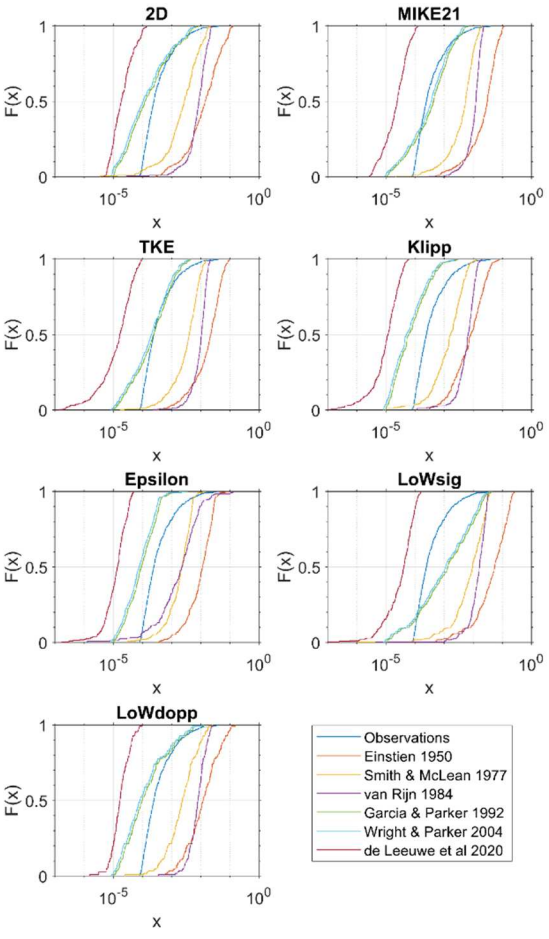

Figure 7. Distributions of measured and predicted near bed suspended sediment concentrations. X axis is concentration in kg m-3 and the y axis is the cumulative distribution of measurements.

4 DISCUSSION

Given the complex bathymetry of the site, and the additional drag produced from the lander and cable during ebb tides, it is perhaps surprising that the 2D methods of estimating bed shear stress (used with Garcia and Parker 1991) estimated near-bed suspended sediment concentrations similarly well to the TKE method which used near bed turbulence measurements. The data from the upward facing Sig1k (used to drive the 2D method) implicitly incorporates both the Eulerian and Lagrangian effects of the bedforms and sand bank on tidal forcing and local flow velocity – something which not all models incorporate. The result highlights that if given good-quality data, the 2D methods do work well.

Given that the TKE performs roughly as well as the 2D methods, one could conclude that near bed turbulence effects on suspending sediment in this deployment are minimal. The higher near-bed suspended sediment concentrations (Figures 4 and 5) would indicate that this does not seem likely.

The highest concentration of near-bed suspended sediment, which were underpredicted by any of the Garcia and Parker family of models (Figure 6), is likely due to the enhanced suspension from the cable and the instrument frame (Figure 3). One of the assumptions of the method is that there is a local equilibrium in the suspension (i.e., no erosion and deposition) which may not be true here as the seabed inevitably adjusted to the presence of the frame. The turbulence generated by the frame appears to have not been fully captured by the near-bed instruments in a way which would lead to equally high predictions of suspended sediment concentrations via the turbulence-based method.

5CONCLUSIONS

At present we conclude that for estimating suspended sediment concentrations (and thus bed shear stresses), both the depth averaged methods, and the near bed method (via TKE) are about as good in this environment. The Law of the wall-based methods should be avoided. We will investigate next how of the performance of the 2D models is due to 1) the velocities being driven by the ADCP data 2) the low noise of the input compared to the nosier (but theoretically more accurate) near bed turbulence methods.

6ACKNOWLEDGEMENTS

This work was funded by the EPSRC Supergen ORE Flexible Fund grant FF2020-1095 and the ECOWind-ACCELERATE project (NE/X008886/1). AJC and RJSW also acknowledge provision of matching funds from the HR Wallingford strategic Scour Research Programme. The team thanks Ben Powell, Aled Owen, and the crew of the RV Prince Madog for facilitating this fieldwork under difficult working conditions due to COVID-19 restrictions.

7REFERENCES

Baas, J. H., van Dam, R. L., & Storms, J. E. a. (2000). Duration of deposition from decelerating high-density turbidity currents. Sedimentary Geology, 136(1–2), 71–88. https://doi.org/10.1016/S0037-0738(00)00088-9

de Leeuw, J., P. Lamb, M., Parker, G., Moodie, A. J., Haught, D., G. Venditti, J., & Nittrouer, J. A. (2020). Entrainment and suspension of sand and gravel. Earth Surface Dynamics, 8(2), 485–504. https://doi.org/10.5194/esurf-8-485-2020

Dey, S., Ali, S. Z., & Padhi, E. (2020). Hydrodynamic Lift on Sediment Particles at Entrainment: Present Status and Its Prospect. Journal of Hydraulic Engineering, 146(6), 03120001. https://doi.org/10.1061/(asce)hy.1943-7900.0001751

Dyer, K. R. (1986). Coastal and estuarine sediment dynamics. John Wiley & Sons.

Egan, G., Cowherd, M., Fringer, O., & Monismith, S. (2019). Observations of Near-Bed Shear Stress in a Shallow, Wave- and Current-Driven Flow. Journal of Geophysical Research: Oceans, 124(8), 6323–6344. https://doi.org/10.1029/2019JC015165

Einstein, H. A. (1950). The bed-load function for sediment transportation in open channel flows. Technical report 1026, Soil Conservation Service.

Garcia, M., & Parker, G. (1991). Entrainment of Bed Sediment into Suspension. In Journal of Hydraulic Engineering (Vol. 117, Issue 4, pp. 414–435). https://doi.org/10.1061/(ASCE)0733-9429(1991)117:4(414)

Herbert, C. M., Alexander, J., & Martínez de Álvaro, M. J. (2015). Back-flow ripples in troughs downstream of unit bars: Formation, preservation and value for interpreting flow conditions. Sedimentology, 62(7), 1814–1836. https://doi.org/10.1111/sed.12203

Klipp, C. (2018). Turbulent friction velocity calculated from the Reynolds stress tensor. Journal of the Atmospheric Sciences, 75(4), 1029–1043. https://doi.org/10.1175/JAS-D-16-0282.1

Lefebvre, A., Herrling, G., Becker, M., Zorndt, A., Krämer, K., & Winter, C. (2022). Morphology of estuarine bedforms, Weser Estuary, Germany. Earth Surface Processes and Landforms, 47(1), 242–256. https://doi.org/10.1002/esp.5243

McLean, S. R., Wolfe, S. R., & Nelson, J. M. (1999). Spatially averaged flow over a wavy boundary revisited. Journal of Geophysical Research: Oceans, 104(C7), 15743–15753. https://doi.org/10.1029/1999jc900116

Nowell, A., & Church, M. A. (1979). Turbulent flow in a depth-limited boundary layer. Journal of Geophysical Research-Oceans, 84(C8), 4816–4824.

Rijn, L. van. (2007). Unified view of sediment transport by currents and waves. II: Suspended transport. Journal of Hydraulic Engineering, 133(6). http://ascelibrary.org/doi/abs/10.1061/(ASCE)0733-9429(2007)133:6(668)

Salim, S., Pattiaratchi, C., Tinoco, R. O., & Jayaratne, R. (2018). Sediment Resuspension Due to Near-Bed Turbulent Effects: A Deep Sea Case Study on the Northwest Continental Slope of Western Australia. Journal of Geophysical Research: Oceans, 123(10), 7102–7119. https://doi.org/10.1029/2018JC013819

Scannell, B. D., Rippeth, T. P., Simpson, J. H., Polton, J. A., & Hopkins, J. E. (2017). Correcting surface wave bias in structure function estimates of turbulent kinetic energy dissipation rate. Journal of Atmospheric and Oceanic Technology, 34(10), 2257–2273. https://doi.org/10.1175/JTECH-D-17-0059.1

Smith, J. D., & McLean, S. R. (1977). Spatially averaged flow over a wavy surface. Journal of Geophysical Research, 82(12), 1735–1746.

Soulsby, R. (1997). Dynamics of Marine Sands. Thomas Telford Publications.

Soulsby, R. L., & Dyer, K. R. (1981). The form of the near-bed velocity profile in a tidally accelerating flow. Journal of Geophysical Research, 86(C9), 8067. https://doi.org/10.1029/JC086iC09p08067

Tang, C., Li, Y., Acharya, K., Du, W., Gao, X., Luo, L., & Yu, Z. (2019). Impact of intermittent turbulent bursts on sediment resuspension and internal nutrient release in Lake Taihu, China. Environmental Science and Pollution Research, 26(16), 16519–16528. https://doi.org/10.1007/s11356-019-04847-2

Tennekes, H., & Lumley, J. L. (1972). A first course in turbulence. MIT press.

Tsai, C. W., & Huang, S. H. (2019). Modeling Suspended Sediment Transport Under Influence of Turbulence Ejection and Sweep Events. Water Resources Research, 55(7), 5379–5393. https://doi.org/10.1029/2018WR023493

Van den Berg, J. H., & Van Gelder, A. (1993). A new bedform stability diagram, with emphasis on the transition of ripples to plane bed in flows over fine sand and silt. Special Publication of the International Association of Sedimentologists, 17, 11–21.

Wright, S., Parker, G., & Asce, M. (2005). Simplified Stratification Model. Journal of Hydraulic Engineering, 130(8), 796–805. https://doi.org/10.1061/(ASCE)0733-9429(2004)130